

CrossMark
click for updatesCite this: *J. Mater. Chem. C*, 2015, 3,
664

Synthesis and nonvolatile memristive switching effect of a donor–acceptor structured oligomer

Cheng Wang,^{†a} Gang Liu,^{†b} Yu Chen,^{*ac} Run-Wei Li,^{*b} Wenbin Zhang,^b Luxin Wang^a and Bin Zhang^a

As promising nonlinear dynamic electronic devices with widespread potential applications in computer data storage and neuromorphic implementations, memristors have attracted tremendous attention in both materials science and condensed-matter physics. In this work, self-rectified memristive behavior was for the first time observed in a highly soluble metal-free all-organic material containing electron-rich fluorene and dithieno[3,2-*b*:2',3'-*d*]pyrrole moieties in the oligomer mainchain as conjugated channels for charge carriers and electron-poor 9,9-bis(3,4-bis(3,4-dicyanophenoxy)phenyl)phenyl side chains in the C-9 position of the fluorene units (hereafter denoted as "PFD-8CN"). Electrical conductance of PFD-8CN can be switched between two states with a rectification ratio of ~ 10 , incrementally and repeatedly. Non-linear transmission characteristics of a biological synapse are also realized through consecutive multilevel conductance switchings. The novel electrical response of the device arises from electric field-induced charge transfer interactions in the donor–acceptor structured oligomer. The development of the organic memristor may offer new opportunities for the construction of molecular electronics that can greatly enhance the performance of modern computer systems.

Received 10th October 2014
Accepted 9th November 2014

DOI: 10.1039/c4tc02285h

www.rsc.org/MaterialsC

Introduction

Designing novel device concepts and discovering new functionalities through rational design and synthesis of novel functional materials are always major tasks for chemists and material scientists. Over the past few decades, great efforts have been devoted to developing innovative technologies that exploit new concepts and materials for the evolution of electronics.^{1–4} As the fourth passive circuit element beyond the fundamental resistor, capacitor and inductor, the memristor was originally envisioned by L. Chua⁵ in 1971 and considered capable of mimicking the function of a mammalian synapse with the ability to learn and memorize new information, and to allow powerful and energy-efficient processing capability for complex open-ended computing tasks. After having being proposed for thirty seven years, the missing memristor was first physically implemented by physicists and electrical engineers in 2008 with metal oxide crossbar arrays.⁶ Emulation of the learning and memorizing ability of synapses and the connected neighboring

neurons, *viz.* short term and long term memory behavior, is simply realized through spike-dependent incremental resistance (or conductance), switching characteristics in two-terminal devices.^{7,8} According to the redefinition of L. Chua in 2011,⁹ all two-terminal nonvolatile resistance switching memory devices are memristors, regardless of the device material or the physical operating mechanisms.

Organic and oligomeric functional materials carry inherent compatibility with living tissues for the construction of biologically implantable neuromorphic memristors. The wide scope of organic chemistry and vast reservoir of functional molecules also allow fine tuning of the structural, chemical and electronic properties of the switching media. Nevertheless, less attention has been paid to the development of high-performance organic memristors. In pioneering works on organic memristors, oligomeric and polymeric materials were used either in metal-containing or multi-component redox systems.^{10,11} The involvement of metal ions or foreign species, however, may not always give rise to uniformly dispersed and compatible components, and may lead to gradual degradation of the functioning oligomers, therefore resulting in less favorable performance of the memory behaviors. To solve such compatibility and stability issues, a solution-processable oligomer that can provide the necessary electronic properties within a single molecule and still possess good chemical, mechanical and morphological characteristics is desired for memristor device applications. Benefiting from the well-developed areas of organic electronics, in particular, the photovoltaic

^aKey Laboratory for Advanced Materials, Institute of Applied Chemistry, East China University of Science and Technology, 130 Meilong Road, Shanghai 200237, China. E-mail: chentangyu@yahoo.com

^bKey Laboratory of Magnetic Materials and Devices, Ningbo Institute of Material Technology and Engineering, Chinese Academy of Sciences, 1219 West Zhongguan Road, Ningbo, Zhejiang 315201, China. E-mail: runweili@nimte.ac.cn

^cThe State Key Laboratory of ASIC & System, Fudan University, 220 Handan Road, Shanghai 200433, China

[†] These authors contribute equally to this work.

and bistable switching devices,¹² rational design and synthesis of memristive oligomers can be made possible, both theoretically and experimentally.

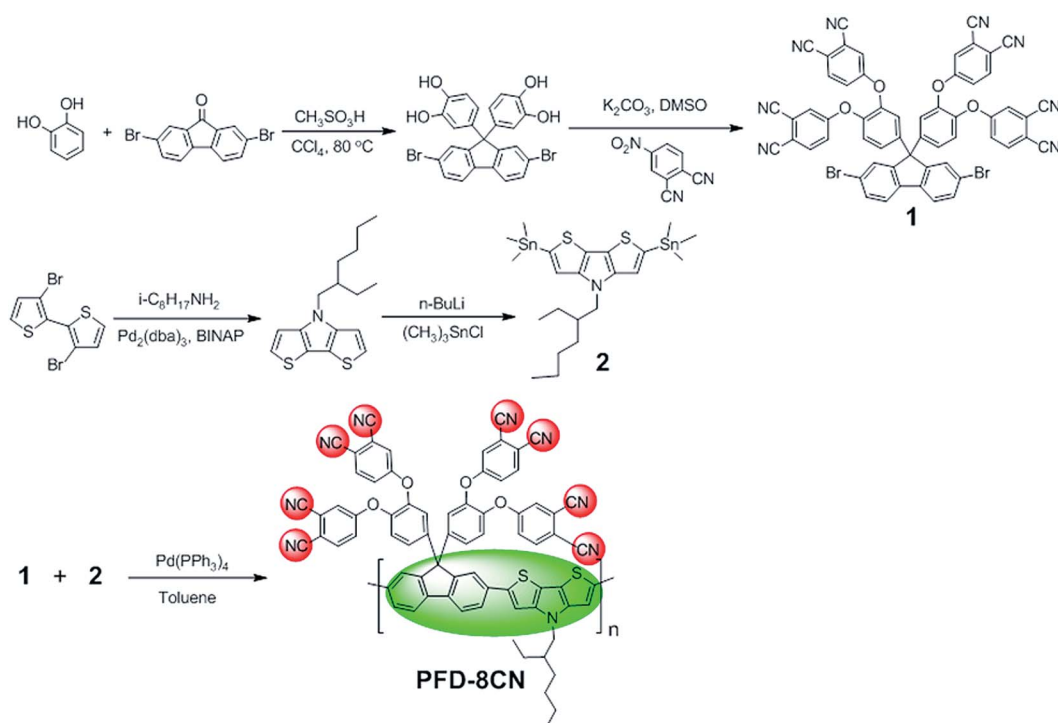
Basically, the molecular structure and memristive properties of organic materials can be fine-tailored by functionalizing them with electron donors (D) and acceptors (A)¹³ of different strengths, spacer moieties of different steric effects for the electroactive pendant groups, or nanostructured electroactive materials. By utilizing coplanar fused aromatic molecules as building blocks, which can form a highly crystalline thin film microstructure domain leading to efficient charge transport, one can easily achieve high-performing organic/oligomeric semiconducting materials. As an analogue of the carbazole molecule, dithieno[3,2-*b*:2',3'-*d*]pyrrole (DTP) and its derivatives have emerged as popular building blocks for the construction of oligomeric semiconducting materials due to their good structural planarity and strong electron-donating ability arising from nitrogen atoms.^{14–16} In this work, we synthesized a novel DTP and fluorene-based D–A type conjugated oligomer, PFD-8CN, as shown in Scheme 1. The utilization of coplanar donor molecule of DTP, in conjunction with the hole-transporting fluorene moiety,¹⁶ can lead to enhanced intermolecular packing, a lower energy bandgap and higher electrical conductance for fast access of the programmed states. The presence of multiple electron accepting cyano (–CN) moieties may tune the CT interaction and the transport behavior of the oligomer successively. Therefore, a stable and incrementally switching of the material conductance is observed in the tantalum/oligomer/platinum structure with a high OFF state conductivity over 100 S m^{–1} and an interesting self-rectifying nature for over 700 cycles.

Moreover, this oligomer demonstrates learning and memorizing capability with its conductance showing multilevel characteristics that are strongly dependent on the history of the applied electrical fields, and bringing neuromorphic computing closer by imitating the performance of synapses. Experimental observation and molecular simulation indicate that the memristive switching is related to the formation of electrically more conductive CT complexes of the cationic DTP⁺ and anionic CN[–] pairs.

Experimental

General

Weight-average (M_w) and number-average (M_n) molecular weights of the oligomer were determined with a Waters 2690 gel permeation chromatography (GPC), using monodispersed polystyrene samples as the molecular weight standards and tetrahydrofuran (THF) as the eluent. Fourier transform infrared (FTIR) spectra were measured on a Nicolet Nagma-IR 550 spectrophotometer by dispersing the samples in KBr pellets. ¹H nuclear magnetic resonance (¹H NMR) spectra were measured on a 400 MHz Bruker Advance 500 NMR spectrometer with CDCl₃ as the solvents and tetramethylsilane (TMS) as the internal standard. UV-visible (UV-vis) absorption spectra of the oligomer solution and film samples were obtained on a Shimadzu UV-2540 spectrophotometer. Steady-state fluorescence spectra were measured on a HORIBA-JOBIN-YVON Fluoromax-4 spectrofluorophotometer. The sample for the fluorescence measurement was dissolved in dry solvents, filtered and transferred to a long quartz cell, where it was capped and degassed



Scheme 1 Synthesis of PFD-8CN.

with ultrapure nitrogen for 10 min before measurement. Cyclic voltammetric measurement was performed on a CHI 650D electrochemical workstation (Chenhua, Shanghai, China) using a three-electrode cell under a nitrogen atmosphere. The oligomer film coated on a Pt disk electrode (working electrode) was scanned anodically and cathodically in an electrolyte solution of tetrabutylammonium perchlorate ($n\text{-Bu}_4\text{NClO}_4$) in acetonitrile (0.1 M), with Ag/AgCl and a platinum wire as the reference and counter electrode, respectively. The Pt working electrode was polished with BAS polishing alumina suspension and rinsed with acetone before use.

Synthesis and characterization

The synthesis of monomers and the oligomer were carried out in an ultrapure nitrogen atmosphere following the procedure as shown in Scheme 1. The monomers **1** and **2** were synthesized according to the literature.^{17,18} The PFD-8CN oligomer was synthesized through Stille coupling reaction. In general, 135 mg of **1** (0.22 mmol) and 209 mg of **2** (0.20 mmol) were dissolved in 8 mL anhydrous toluene in a 25 mL Schlenk tube and degassed with nitrogen for 15 min. After adding 10 mg of Pd(PPh₃)₄ into the Schlenk tube, the reaction mixture was degassed for another 15 min and then heated to 120 °C for 48 h. Upon being cooled to room temperature, the crude product was collected by precipitation in methanol (100 mL) with vigorously stirring. The as-received solid was re-dissolved in CHCl₃ and ran through a siliceous earth column quickly to remove the metal catalyst residue. Then the crude oligomer was subjected to Soxhlet extraction with acetone, hexane, and CHCl₃ sequentially to remove the unreacted monomers and the trace catalyst. CHCl₃ portion was concentrated and re-precipitated in methanol, and dried under vacuum overnight to obtain the dark-red target oligomer (PFD-8CN) with a yield of 65.1% (153 mg). $M_n = 4.52 \times 10^3$ (four repeating units per molecule), $M_w/M_n = 1.13$. ¹H-NMR (CDCl₃, 400 MHz): δ /ppm = 7–8 (m, 26H), 4.08 (m, 2H), 1.97 (m, 1H), 1.31 (m, 8H), 0.90 (m, 6H). The resultant oligomer does not show a glass-transition temperature when heated up to 350 °C. T_d (5%) = 379 °C (in nitrogen). All chemicals were purchased from Aldrich and used without further purification. Organic solvents were purified, dried and distilled under dry nitrogen.

Fabrication and measurements

The electrical properties of PFD-8CN were evaluated in **Ta/oligomer/Pt sandwich structures**. The Pt/Ti/SiO₂/Si substrates were pre-cleaned with ethanol, acetone and isopropanol in an ultrasonic bath, each for 20 min in that order. After being filtered through a polytetrafluoroethylene (PTFE) membrane micro-filter with a pore size of 0.45 μm , a 50 μL cyclohexanone solution of PFD-8CN (1.0 wt% oligomer) was spin-coated onto the substrates at a spinning speed of 400 rpm for 12 s and then 2000 rpm for 40 s, followed by vacuum-drying at 80 °C overnight. The thickness of the oligomer film was about 100 nm as measured by spectroscopic ellipsometer (model M2000DI, Woollam). Ta top electrodes with a diameter of 100 μm and thickness of 50 nm were deposited on the film surface at room temperature under reduced pressure (below 10^{-5} Pa) by E-beam

evaporation. The devices were characterized under ambient conditions, using a Keithley 4200 semiconductor characterization system equipped with a Keithley 3402 pulse generator, in both the voltage sweeping and pulse mode. The sweeping step was 0.01 V. A compliance current (CC) presetting of 1 mA was used to avoid over-striking or permanent breakdown of the sample. An atomic force microscopy (Dimension V, Veeco) equipped **with a conducting cantilever coated with Pt/Ir** was employed for the conductive atomic force microscopic (C-AFM) measurements of the oligomer/Pt devices. During the measurement, **the tip was always grounded while a bias voltage was applied on the Pt film.**

Molecular simulation

Calculations of the optimized geometry and electronic structure, including the dipole moment, electrostatic potential (ESP) surface, as well as HOMO and LUMO of the basic unit of the PFD-8CN oligomer were carried out on a Compaq ES40 super-computer using the Gaussian 09 program package and **DFT calculations at the B3LYP/6-31G(d) level.**¹⁹ Based on the ground state calculations using the above-mentioned method, the corresponding electronic properties of the basic unit of PFD-8CN in the excited (or, ON) state were calculated using the configuration interaction approach involving the single-electron excitation method at the CIS/6-31G(d) level with the Gaussian 09 program package.^{20,21}

Results and discussion

PFD-8CN was synthesized through the palladium-catalyzed coupling reaction of monomers **1** and **2** in the presence of tetrakis(triphenylphosphine)palladium(0) as the catalyst. This oligomer is soluble in many common organic solvents. By GPC analysis against a linear polystyrene standard, PFD-8CN was found to have M_n of 4.52×10^3 (four repeating units per molecule), and a polydispersity of 1.13. The chemical structure of PFD-8CN can be verified through ¹H-NMR and Fourier transform infrared (FTIR) spectroscopy. Its ¹H-NMR spectrum reveals proton signals of the alkyl side chain of the DTP donor with the chemical shifts of 4.08 (m, 2H), 1.97 (m, 1H), 1.31 (m, 8H), and 0.90 (m, 6H) ppm, as well as that of the benzene rings at δ /ppm = \sim 7–8 (m, 26H) for the conjugated D–A system. The moderate absorption peak at 2230 cm^{-1} appeared in the IR spectrum can be attributed to the stretching vibration mode of the cyano groups, while the absorption peaks at 1597, 1488 and 1407 cm^{-1} , as well as that at 1260 and 1100 cm^{-1} , are associated with the skeleton and C–H bending vibrations of the aromatic rings, respectively.

PFD-8CN demonstrates a distinctive asymmetric resistive switching behavior at room-temperature, as shown in the current–voltage (I – V) characteristics of Fig. 1a. Before the electrical measurements, a 100 nm thin film of PFD-8CN was spin-coated from the solution onto a grounded Pt/Ti/SiO₂/Si substrate. A metal/insulator/metal sandwiched structure was formed and tested with an evaporated tantalum pad of 100 μm in diameter as the top electrode (inset of Fig. 1a). The biased-

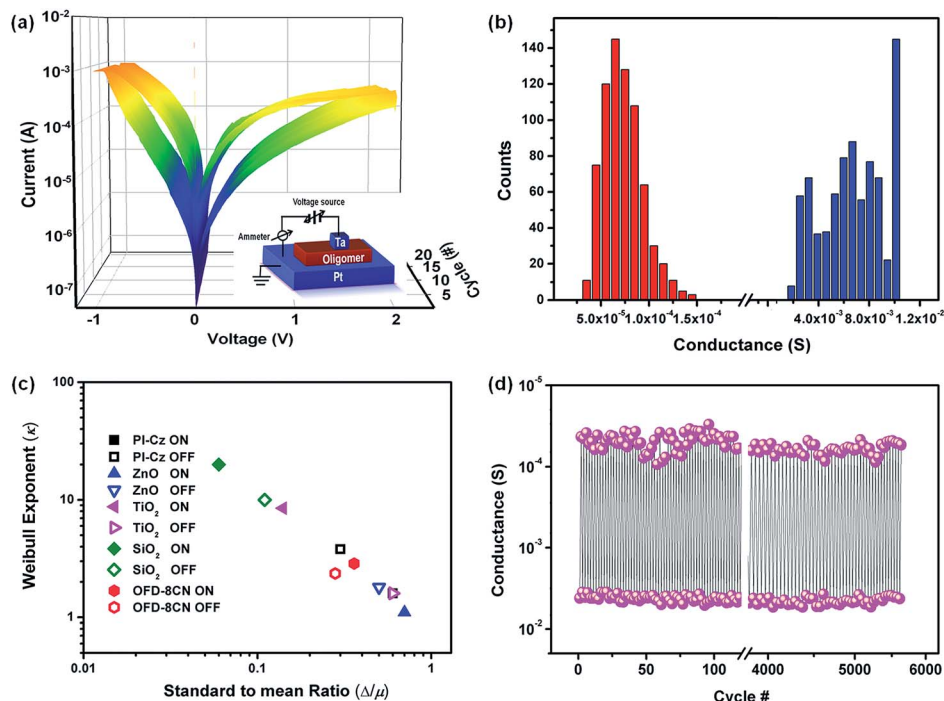


Fig. 1 Memristive characteristics of PFD-8CN. (a) 3D current–voltage profile of PFD-8CN in a metal/oligomer/metal sandwich structure; (b) distribution of sample conductance in both the OFF and ON states; (c) Weibull exponent (k) versus standard deviation to mean ratio (Δ/μ) for the ON and OFF state conductance of PFD-8CN and reported devices (green,²⁶ pink,²⁸ blue,²⁹ magenta³⁰); and (d) switching cyclability of the sample under pulse operation mode. Inset of (a) is the schematic illustration of Ta/oligomer/Pt structure.

sweeping voltage was applied across the sandwich structure, with a compliance current presetting of 1 mA employed to avoid over striking and permanent breakdown of the switching media. Initially present in the OFF state, PFD-8CN shows a moderate conductivity of $100 \text{ S m}^{-1} \sim 800 \text{ S m}^{-1}$, probably arising from the ground state charge transfer interaction (see later section for detail discussion). This conductivity value is comparable with that of the chemically-doped conducting polymers, and is favorable for the fast reading of the device states. By sweeping the voltage in the direction of $0 \text{ V} \rightarrow -1 \text{ V} \rightarrow 0 \text{ V} \rightarrow 2 \text{ V} \rightarrow 0 \text{ V}$, PFD-8CN can be switched smoothly between two resistance states with a stable ON/OFF ratio of ~ 10 (read at $\pm 0.5 \text{ V}$). Differing from the bistable resistive switching showing abrupt resistance or conductance jumps, the electrical transition observed here demonstrates a smoother tuning of the sample conductance during the voltage sweeping processes. Together with a “pinch-off” feature in the I - V curve (Fig. 2a), this resistive switching phenomenon is definitely the characteristic of a memristor device.²² Interestingly, a self-rectifying effect with the rectification ratio of ~ 10 in both ON and OFF states, which may arise from the Schottky barrier for charge carrier injection at the Ta/PFD-8CN interface (see later section for details), was also observed in the oligomer. Although the self-rectifying effect of the present PFD-8CN device is relatively less obvious, it still provides a simple but effective approach to eliminate the incorporation of additional control elements to solve the cross-talking problem in crossbar-structured devices, or to emulate the single-direction information transmission in

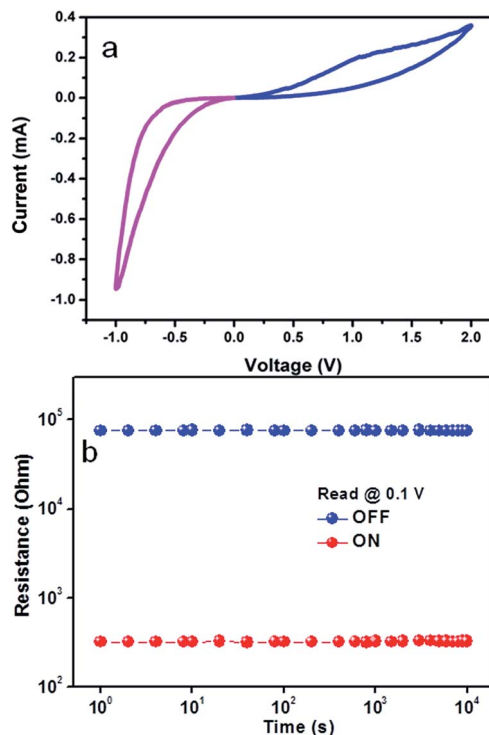


Fig. 2 (a) 2D current–voltage profile of the PFD-8CN memristive device that demonstrates a “pinch-off” characteristic; and (b) retention capability of the PFD-8CN memristive device in both the ON and OFF states.

biological systems.^{23–25} Further improvement of the self-rectifying effect may be further achieved by fine-tuning the electronic structure of the electroactive materials. The atmospheric moisture or oxygen may cause minor fluctuation in the device resistances, but are unlikely to be the governing factors that induce the observed resistive switching in PFD-8CN devices.^{10,26,27}

To investigate the uniformity of the conductance-switching behavior, cyclic sweeping operations of the Ta/oligomer/Pt device was performed. A narrow distribution of the device conductance at both the OFF and ON states in over 700 switching cycles is demonstrated in Fig. 1b. Weibull distribution is employed to further evaluate the uniformity of the resistive switching parameters by the following equation:

$$F(x) = 1 - \exp(-(x/x_0)^k) \quad (1)$$

where x is a random variable, x_0 is the scale parameter of the distribution of x , k is defined as the Weibull exponent and $F(x)$ is the cumulative probability of finding a randomly-distributed variable (a switching parameter in the present work) below x relative to a scaling constant x_0 . The Weibull exponent can be correlated with the standard deviation (Δ) to mean (μ) ratio (Δ/μ) using the following equation:

$$\Delta/\mu = \frac{[\Gamma(1 + 2/k) - \Gamma^2(1 + 1/k)]^{1/2}}{\Gamma(1 + 1/k)} \quad (2)$$

where Γ is the Gamma function. The plots of Weibull exponent k as a function of the standard deviation to mean ratio Δ/μ , for the conductance of the PFD-8CN and other reported devices, are shown in Fig. 1c, where a larger Weibull exponent corresponds

to a narrower distribution of the variable.^{28,29} In comparison, the PFD-8CN devices exhibit k and Δ/μ values comparable to that of the reported devices with either oxide or organic materials as the switching media. The standard deviation (Δ) to mean (μ) ratios of the OFF and ON state conductance are found to be 0.283 and 0.364, respectively, which are lower than or comparable to that of the other reported devices.^{28,30–32} Moreover, the conductance of the oligomer can be well maintained under a constant read voltage stress of 0.1 V for 10^4 s, or switched between the ON and OFF states by pulse operation for 6000 cycles, respectively (Fig. 1d and 2b), again suggesting the excellent uniformity and stability in the switching behavior of PFD-8CN.

The other characteristics of a synaptic memristor is that its synaptic weight, usually defined as the conductance of the two terminal device, can be modulated and memorized using consecutive spikes. As shown in Fig. 3a and b, the conductance of the PFD-8CN device can be decreased continuously, with the corresponding positive (0 V to 2 V) and negative (0 V to -1 V) voltage sweeps executed consecutively. A better illustration of the degressive change of the oligomer memristor's synaptic weight, demonstrated as the sweeping voltage and responding current *versus* time characteristics, as well as the device conductance obtained at the end of each sweep, are plotted in Fig. 3c. It is interesting that a single negative or positive sweep can increase or decrease the device conductance (or synaptic weight), respectively, while both the consecutive negative and positive sweeps serve as synaptic spikes to inhibit the bio-mimicking memristor devices, where similar phenomena observed in biological synapse are defined as nonlinear transmission characteristics. The reason for consecutive negatives

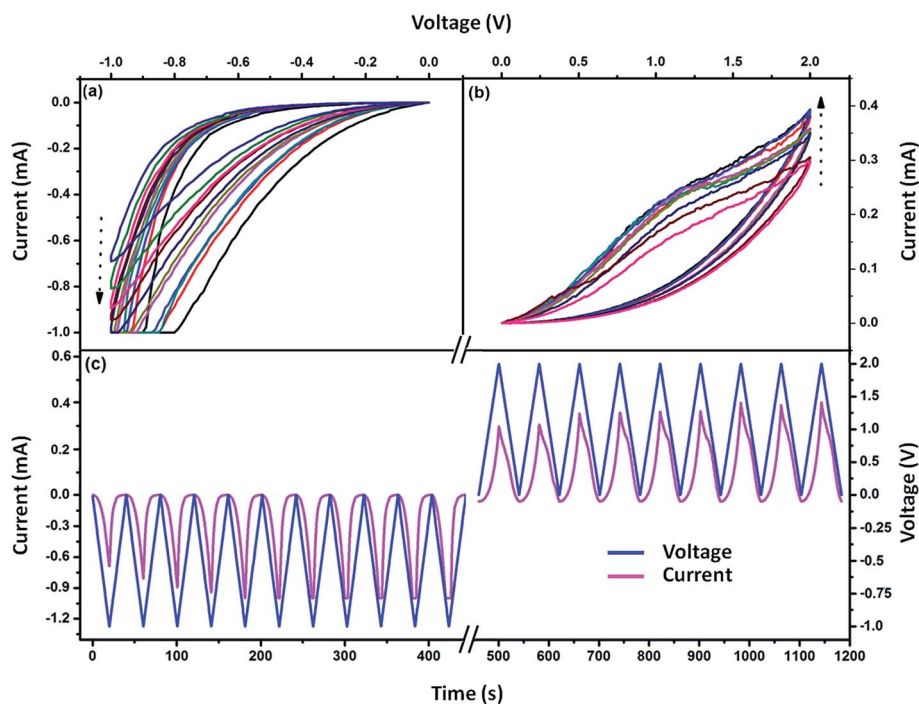


Fig. 3 Nonlinear transmission characteristics of the PFD-8CN memristor. (a and b) Current–voltage characteristics of the memristor at negative and positive biased sweeps; and (c) current and voltage *versus* time profiles of the memristor plotted from the data in (a) and (b).

acting as the inhibitory synaptic spikes is still not clear at the moment.

The switching mechanism of the oligomer is proposed as charge transfer enhanced conductance in the thin solid films, and is verified *via* both theoretical and experimental analysis. It is noteworthy that PFD-8CN sample demonstrate charge transferred nature at ground state. In dilute solution, PFD-8CN shows a moderate optical absorption peak at 280 nm, which can be assigned to the π - π^* transition of the conjugated backbone (Fig. 4a). Intramolecular CT characteristics can be evidenced from the strong absorption in the wavelength range of 400 to 600 nm, ascribed to the coupling between the n - π^* and π - π^* transitions of the *N*-aryl rings and the pendant cyano moieties. With an increase in the solvent polarity, the charge separated state (or, dipole moment) of the D-A macromolecule will get

stabilized notably through solute-solvent interaction, lowering the energy gap between the ground and the CT states, resulting in a red-shift of the optical absorption maximum consequently. Therefore, the observed bathochromic (or positive solvatochromic) phenomena in PFD-8CN also confirm the occurrence of charge transfer interaction in the ground state. When the oligomer concentration is increased in the chloroform solution, additional absorption shoulder associated with intermolecular (charge transfer) interaction between neighboring oligomer chains is observed at \sim 500 nm (Fig. 4c). This absorption shoulder, together with the strong CT peak, merges into a single broader band when PFD-8CN is cast into thin films, suggesting that the intermolecular CT interaction has been further intensified in the solid state, where the rigid-rod oligomer chains are stacked more closely to give an extended π - π

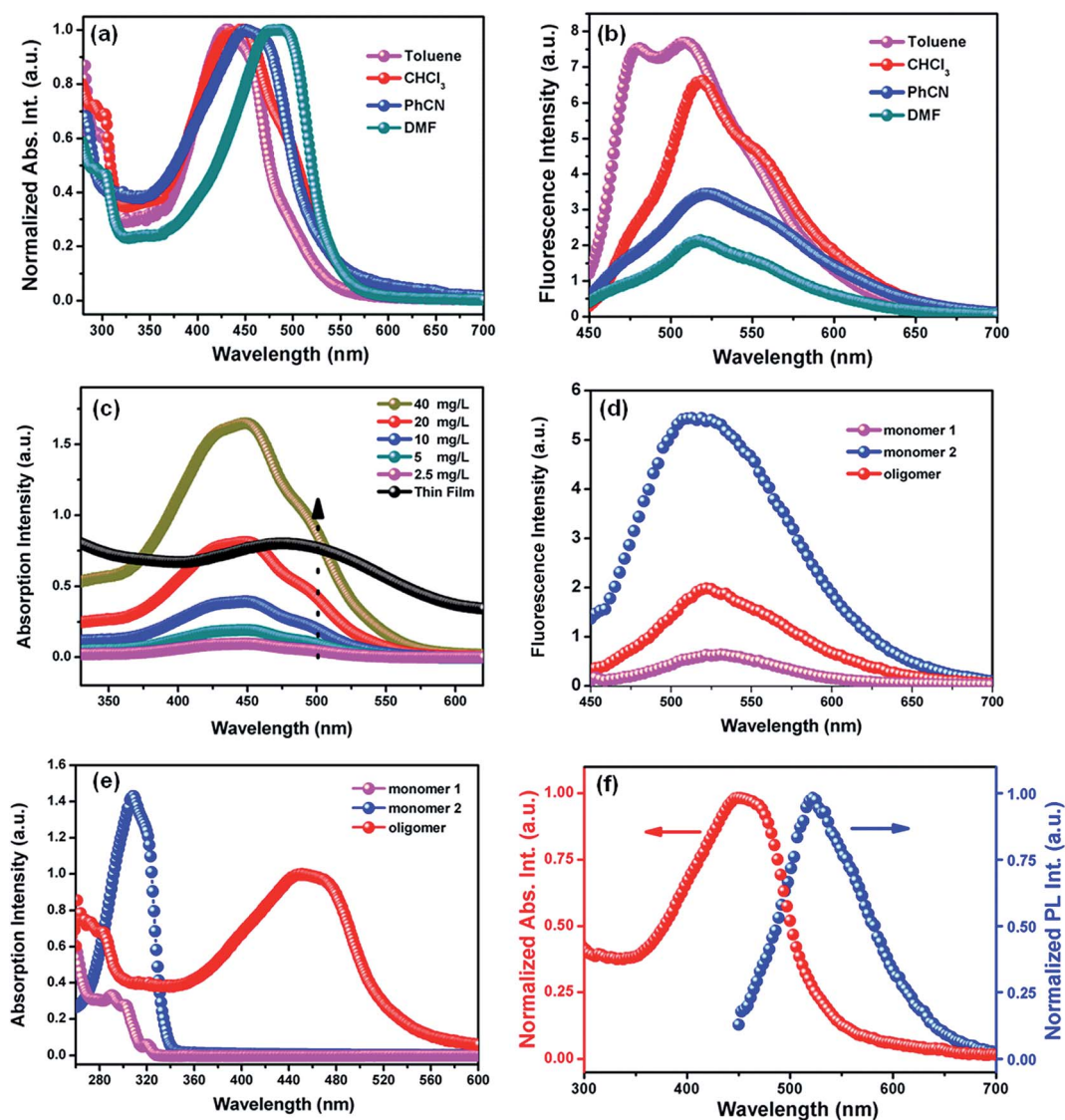


Fig. 4 UV-vis absorption (a) and fluorescence (b), $\lambda_{\text{ex}} = 440$ nm) spectra of PFD-8CN in different organic solvents; (c) UV-vis absorption spectra of PFD-8CN in solid thin film and in chloroform solution with different concentrations; (d) fluorescence spectra of the monomers 1, 2 and PFD-8CN in chloroform, $\lambda_{\text{ex}} = 440$ nm; (e) UV-vis absorption spectra of the monomers 1, 2 and PFD-8CN in chloroform; and (f) UV-vis absorption and fluorescence spectra of PFD-8CN in chloroform. Concentration: $\sim 1 \mu\text{g L}^{-1}$.

stacking between the donor and acceptor unities. However, such aggregates are not efficient due to the large amount of pendant groups tethered to the C-9 position of the fluorene unit, therefore hindering the coplanar association of the aromatic backbone, and resulting in the unchanged wavelength of the CT absorption maximum.

Given the donor–acceptor conjugation structure of the PFD-8CN oligomer, intramolecular interaction is further explored through photoinduced event studies. Upon being exposed to an excitation light beam of the 440 nm wavelength, the DTP monomer **2** exhibits an intensive emission peak at 512 nm, which is similar to the reported values of the DTP moieties (Fig. 4d), while the monomer **1** with eight CN groups has a much reduced emission at the longer wavelength of 527 nm. In comparison to monomer **2**, the chloroform solution of the PFD-8CN oligomer shows significantly quenched dimeric emission bands of the DTP entities at 517 and 550 nm (Fig. 4b), from which the energy of the singlet state is estimated to be 2.40 eV with the following formula:

$$E_{\text{singlet}} = h \frac{c}{\lambda_{\text{em}}} \quad (3)$$

where h is the Planck constant ($6.62 \times 10^{-34} \text{ m}^2 \text{ kg s}^{-1}$), c is the speed of light ($3 \times 10^8 \text{ m s}^{-1}$) and λ_{em} is the characteristic emission wavelength of the oligomer (517 nm). The fluorescence quantum yield of the PFD-8CN oligomer is only $\sim 4\%$, which is much smaller than that of the other DTP-based materials.³³ The observed fluorescence quenching in PFD-8CN, as well as the poor matching between the emissive spectrum of the DTP donor and the absorption spectrum of the -CN acceptor (Fig. 4e), also indicate the occurrence of CT between the electron donor and the acceptor at ground states. Similar to the bathochromic effect, increasing the polarity of the solvents will stabilize the charge separated state of the oligomer, leading to a quenched, broader and red-shifted emissive spectrum in

the visible region (for instance, 480 nm in toluene, 517 nm in chloroform, 519 nm in benzonitrile and 521 nm in dimethylformamide). The finding that the fluorescence intensity decreases with increasing solvent polarity again suggests the occurrence of electron transfer process from the DTP donor to the -CN acceptor moieties.

By using electrochemical measurements, optical characterization and molecular simulation, the thermodynamics of the charge transfer process in PFD-8CN is further assessed. Cyclic voltammetry (CV) measurements reveal oxidation of the DTP unit with doublet anodic responses at $E_{\text{onset}}(\text{OX}_1) = 0.55 \text{ V}$ and $E_{\text{onset}}(\text{OX}_2) = 1.30 \text{ V}$, respectively.³⁴ As the oligomer film dissolved after being electrochemically oxidized in electrolyte solutions, the reversible reduction of the formed cationic radicals of the electron donating backbone was not detected. Cathodic reduction of PFD-8CN was also observed at -1.79 V . Due to considerable ground-state CT interaction between the DTP donor and the -CN acceptor entities, the oligomer exhibits a low energy bandgap of $\sim 2.34 \text{ eV}$ which well agrees with that ($\sim 2.36 \text{ eV}$) derived from the optical absorption edge of Fig. 4a. Thus, the energy levels of the highest occupied molecular orbital (HOMO) and lowest unoccupied molecular orbital (LUMO) of PFD-8CN are derived to be -4.97 eV and -2.63 eV , respectively. With the working functions of -4.25 eV for Ta and -5.65 eV for Pt,³⁵ respectively, Schottky and Ohmic contacts are formed at the TA/PFD-8CN and PFD-8CN/Pt interfaces accordingly.

According to the Rehm–Weller equations:

$$-\Delta G_{\text{CR}} = E_{\text{onset}}(\text{OX}_1) - E_{\text{onset}}(\text{RED}) + \Delta G_{\text{S}} \quad (4)$$

$$-\Delta G_{\text{CS}} = \Delta E_{0-0} - (-\Delta G_{\text{CR}}) \quad (5)$$

$$\Delta G_{\text{S}} = -e^2/4\pi\epsilon\epsilon_0 R_{\text{CC}} \quad (6)$$

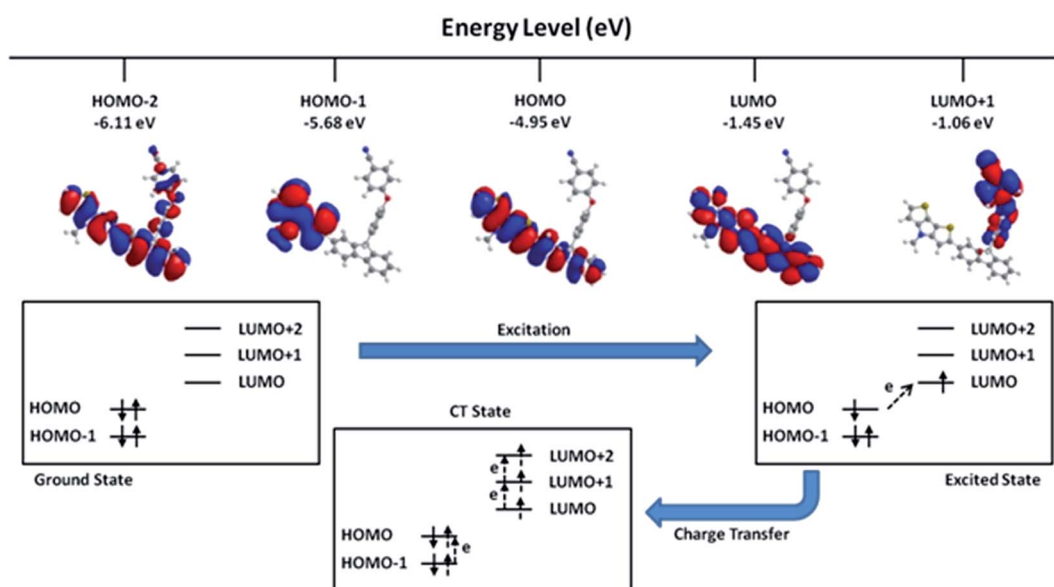
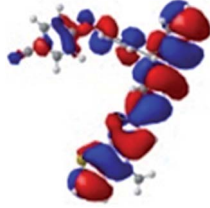
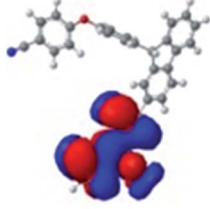
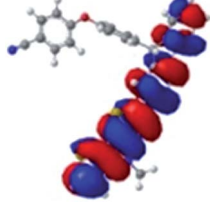
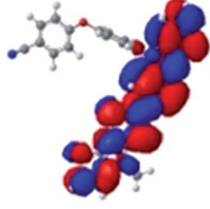
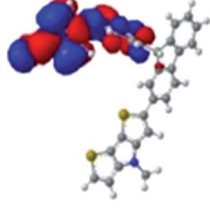
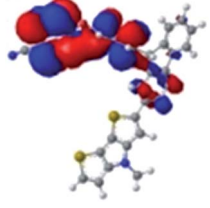
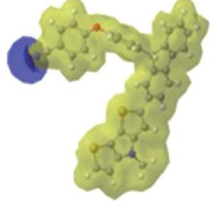
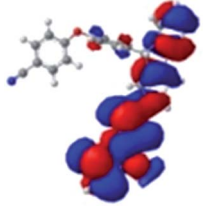
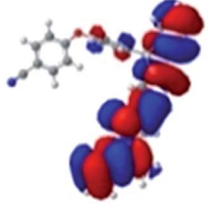
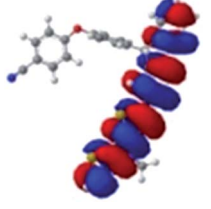
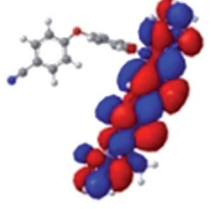
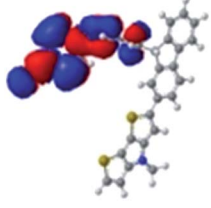
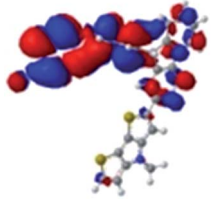
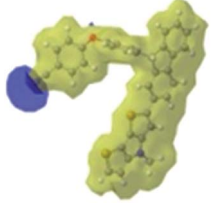


Fig. 5 Plausible electric field-induced electronic transition in PFD-8CN.

Table 1 Simulated distribution of electron clouds in the HOMO and LUMO, ESP surfaces and dipole moments of PFD-8CN in both the ground (OFF) and excited (ON) states

	HOMO - 2	HOMO - 1	HOMO	LUMO	LUMO + 1	LUMO + 2	ESP
Ground state	 -6.11 eV	 -5.68 eV	 -4.95 eV	 -1.45 eV	 -1.06 eV	 -0.68 eV	 7.57 Debye
Excited state	 -8.16 eV	 -8.10 eV	 -6.17 eV	 1.33 eV	 2.87 eV	 3.19 eV	 6.96 Debye

where ΔE_{0-0} is the energy of the 0-0 transition between the lowest excited state and ground state of the donor moiety, and evaluated as 2.52 eV from the intersection of absorbance and fluorescence spectra of PFD-8CN at 493 nm (Fig. 4f), e is the elementary charge (1.6×10^{-19} C), ϵ_0 is the vacuum permittivity (8.85×10^{-12} F m $^{-1}$), ϵ_R is static dielectric constant of the solvent (37.5 for acetonitrile and 4.81 for chloroform, respectively) used for the electrochemical measurements, R_{CC} is the distance between the positive and negative charges in the charge-separated state of PFD-8CN and estimated to be 1.15 nm (distance between the pyrrole nitrogen atom and the cyano nitrogen atom) through Gaussian molecular simulation, the coulombic potential energy between the cation and anion radicals (ΔG_S), as well as the driving forces (ΔG_{CR} and ΔG_{CS} , changes of free Gibbs energy) for the charge recombination and separation processes, are derived as -0.26, -2.08 and -0.44 eV (in chloroform solution), respectively. The negative ΔG_{CS} indicates that the occurrence of the charge-separation process is exothermic and simultaneous to form the $(DTP^{+}-CN^{-})_n$ radical ion pair, while the charge-separated state is metastable with the absolute value of ΔG_{CS} smaller than that of ΔG_{CR} .³⁶ The calculated driving forces are not completely accurate, as PFD-8CN cannot be dissolved in acetonitrile, and the fluorescence spectra obtained in chloroform solution is used instead. Nevertheless, such metastable charge-transferred state may be further enhanced under the stimuli of external electric field, and may be responsible for the observed conductance switching behavior of the PFD-8CN device.

Finally, the plausible electronic scenario of the CT process and conductance switching of the PFD-8CN oligomer is proposed with the assistance of molecular simulation and shown in Fig. 5 and Table 1. To accelerate the simulation process, as well as gaining a better understanding of the electronic transition process, a simplified model of the oligomer with only one pendant phenyl-cyano acceptor moiety was employed for molecular simulation. As shown, both the HOMO and LUMO electrons are located on the DTP-fluorene backbone. The calculated HOMO energy level well agrees with that of the experimental data deduced from the electrochemical measurements, while the difference in the calculated and experimental LUMO energy levels arises from the difference in effective conjugation between the oligomer chain and the basic unit. Under electric stimuli, electrons will accumulate sufficient energy, get easily excited from the HOMO into the LUMO, and then transit to the LUMO + 1 that is associated with the -CN acceptor. Since HOMO - 1, HOMO and LUMO are all distributed along the conjugate backbone, the vacancies in the HOMO and LUMO can be partially compensated by electrons from the HOMO - 2 and HOMO - 1 through energy-decay transition. Consequently, a charge transfer state of the PFD-8CN oligomer has been established. The delocalization of electrons among the HOMO - 1 to LUMO + 1 orbitals gives rise to half-filled energy bands similar to that of the metallic conductors, and switches the device from a low conductance state to a high conductance state with increased amount of effective (free) charge carriers. Upon being transitioned to the first excited state, the separated charges distributed on the DTP donor and the -CN acceptor

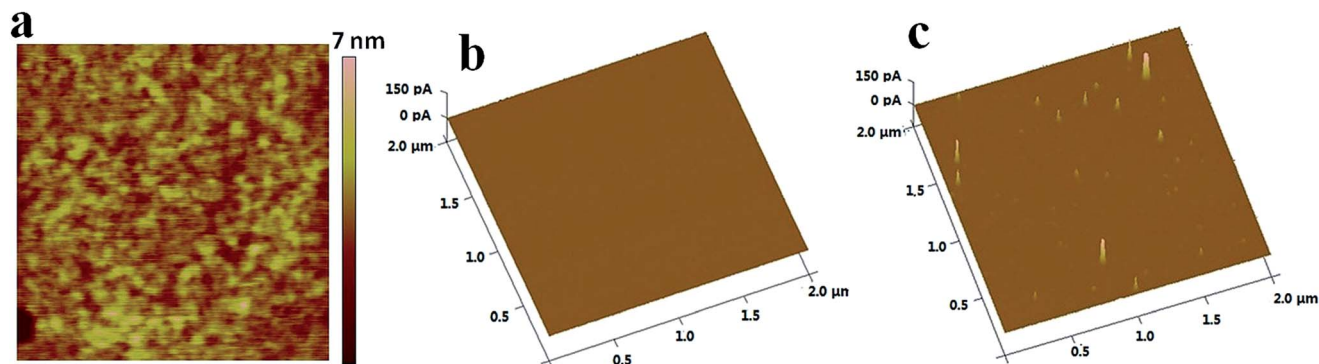


Fig. 6 (a) AFM image of the PFD-8CN film with the scanning size of $2 \times 2 \mu\text{m}^2$; (b) OFF state and (c) ON state C-AFM mapping of the PFD-8CN film with the scanning size of $2 \times 2 \mu\text{m}^2$.

lead to strong attraction between the charged $\text{D}^{+\bullet}-\text{A}^{\bullet-}$ pairs, therefore leading to a stabilized excited state with smaller dipole moment as compared to that of the ground state basic unit of the oligomer, and non-volatile nature of the device memristive behavior. With the inclusion of multiple $-\text{CN}$ acceptors in the repeating unit of the oligomer, charge transfer occurs stepwisely in PFD-8CN, which gives rise to the continuous and consecutive modulation of the device conductance that mimicks the nonlinear transmission characteristics of biological synapses.

As observed by the C-AFM mapping of the oligomer device, the charge-transfer induced conductance switching occurs in localized regions with the diameter of $\sim 20 \text{ nm}$ (Fig. 6). Once such highly conductive regions are formed, the electrical current will flow through them preferentially. Consequently, the other parts of the film are no longer subjected to the applied voltage, and will not undergo any changes to the physico-chemical properties. Considering the much larger device total area and the light beam spot size of either UV-visible absorption or fluorescence spectroscopy, nano-scaled optical diffraction or absorption variation can hardly be detected by the current technique. Complete elucidation of the underlying switching mechanism requires further development in the characterization techniques and instruments, and is of immense importance for the optimization of material structure and device performance.

Conclusions

To the best of our knowledge, this is the first report of memristive effect in a single-component and metal-free organic materials so far. PFD-8CN demonstrates self-rectified memristive behavior with excellent room-temperature reproducibility and stability. Experimental observations and molecular simulation suggest that the unique electrical behavior of PFD-8CN is achieved through a charge transfer process in the donor-acceptor system. Nonlinear transmission characteristic of a biological synapse is also realized through consecutive multi-level conductance switching. The discovery of the memristive in PFD-8CN may provide new possibilities in mimicking the learning and memorizing function of a mammalian synapse in

molecular electronics, and is useful for enhancing the processing capability of modern computer systems with promising parallel capacities.

Acknowledgements

The authors are grateful for the financial support of the National Natural Science Foundation of China (51333002, 21074034, 51303194, 61328402), the Research Fund for the Doctoral Program of Higher Education of China (20120074110004), the State Key Laboratory of ASIC & System of Fudan University (11KF007), the State Key Project of Fundamental Research of China (973 Program, 2012CB933004), the Ningbo Science and Technology Innovation Team (2011B82004), the Ningbo Natural Science Foundation (2013A610031) and the Shanghai Leading Talents program (to Prof. Dr Yu Chen).

References

- 1 R. F. Service, *Science*, 2003, **302**, 556–559.
- 2 Y. Chen, B. Zhang, G. Liu, X. D. Zhuang and E. T. Kang, *Chem. Soc. Rev.*, 2012, **41**, 4688–4707.
- 3 Y. Chen, G. Liu, C. Wang, W. Zhang, R.-W. Li and L. Wang, *Mater. Horiz.*, 2014, **1**, 463–550.
- 4 G. Liu, Y. Chen, R.-W. Li, B. Zhang, E.-T. Kang and C. Wang, *ChemElectroChem*, 2014, **1**, 514–519.
- 5 L. Chua, *IEEE Trans. Circuit Theory*, 1971, **18**, 507–519.
- 6 D. B. Strukov, G. S. Snider, D. R. Stewart and R. S. Williams, *Nature*, 2008, **453**, 80–83.
- 7 J. J. Yang, M. D. Pickett, X. M. Li, D. A. A. Ohlberg, D. R. Stewart and R. S. Williams, *Nat. Nanotechnol.*, 2008, **3**, 429–433.
- 8 J. J. Yang, D. B. Strukov and D. R. Stewart, *Nat. Nanotechnol.*, 2013, **8**, 13–24.
- 9 L. Chua, *Appl. Phys. A*, 2011, **102**, 765–783.
- 10 A. Bandyopadhyay, S. Sahu and M. Higuchi, *J. Am. Chem. Soc.*, 2011, **133**, 1168–1171.
- 11 F. Pincella, P. Camorani and V. Erokhin, *Appl. Phys. A*, 2011, **104**, 1039–1046.
- 12 Q. D. Ling, D. J. Liaw, C. X. Zhu, D. S. H. Chan, E. T. Kang and K. G. Neoh, *Prog. Polym. Sci.*, 2008, **33**, 917–978.

- 13 A. Ajayaghosh, *Chem. Soc. Rev.*, 2003, **32**, 181–191.
- 14 M. Zhang, H. N. Tsao, W. Pisula, C. Yang, A. K. Mishra and K. Müllen, *J. Am. Chem. Soc.*, 2007, **129**, 3472–3473.
- 15 R. E. Palacios, F.-R. F. Fan, J. K. Grey, J. Suk, A. J. Bard and P. F. Barbara, *Nat. Mater.*, 2007, **6**, 680–685.
- 16 J. Peet, J. Y. Kim, N. E. Coates, W. Ma, L. D. Moses, A. J. Heeger and G. C. Bazan, *Nat. Mater.*, 2007, **6**, 497–500.
- 17 X. D. Zhuang, Y. Chen, B. X. Li, D. G. Ma, B. Zhang and Y. X. Li, *Chem. Mater.*, 2012, **22**, 4455–4461.
- 18 M. M. Shi, D. Deng, L. Chen, J. Ling, L. Fu, X. L. Hu and H. Z. Chen, *J. Polym. Sci., Part A: Polym. Chem.*, 2011, **49**, 1453–1461.
- 19 M. J. Frisch, G. W. Trucks, H. B. Schlegel, G. E. Scuseria, M. A. Robb and J. R. Cheeseman, *Gaussian 09 (Revision A.02)*, Gaussian, Inc., Wallingford CT, 2009.
- 20 J. B. Foresman, M. Head-Gordon, J. A. Pople and M. J. Frisch, *J. Phys. Chem.*, 1992, **96**, 135–149.
- 21 J. B. Foresman and A. Frisch, *Exploring chemistry with electronic structure methods*, Gaussian, Inc., 2nd edn, 1996.
- 22 C. H. Huang, J. S. Huang, S. M. Lin, W. Y. Chang, J. H. He and Y. L. Chueh, *ACS Nano*, 2012, **6**, 8407–8414.
- 23 T. W. Kim, D. F. Zeigler, H. L. Yip, H. Ma and A. K. Y. Jen, *Adv. Mater.*, 2012, **24**, 828–833.
- 24 M. E. Bear, B. W. Connors and M. A. Paradiso, in *Neuroscience: Exploring the Brain*, High Education Press, Beijing, 2007, p. 761, ISBN 078-1-7600-38.
- 25 R. C. Atkinson and R. M. Shiffrin, in *The Psychology of Learning and Motivation: Advances in Research and Theory*, Academic Press, New York, 1968, p. 89.
- 26 B. Hu, X. Zhu, X. Chen, L. Pan, S. Peng, Y. Wu, J. Shang, G. Liu, Q. Yan and R.-W. Li, *J. Am. Chem. Soc.*, 2013, **135**, 17408–17411.
- 27 R. R. Kumar, G. Pillai, N. Pekas, Y. Wu and R. L. McCreery, *J. Am. Chem. Soc.*, 2012, **134**, 14869–14876.
- 28 B. J. Choi, A. B. K. Chen, X. Yang and I. W. Chen, *Adv. Mater.*, 2011, **23**, 3847–3852.
- 29 W. Weibull, *J. Appl. Mech.*, 1951, **18**, 293–297.
- 30 W. Y. Chang, K. J. Cheng, J. M. Tsai, H. J. Chen, F. Chen, M. J. Tsai and T. B. Wu, *Appl. Phys. Lett.*, 2009, **95**, 042104.
- 31 Y. C. Yang, F. Pan, Q. Liu, M. Liu and F. Zeng, *Nano Lett.*, 2009, **9**, 1636–1643.
- 32 B. Hu, F. Zhuge, X. Zhu, S. Peng, X. Chen, L. Pan, Q. Yan and R.-W. Li, *J. Mater. Chem.*, 2012, **22**, 520–526.
- 33 S. J. Evenson, M. J. Mumm, K. I. Pokhodnya and S. C. Rasmussen, *Macromolecules*, 2011, **44**, 835–841.
- 34 H. Wong, C. Ko, W. H. Lam, N. Zhu and V. W. Yam, *Chem.–Eur. J.*, 2009, **15**, 10005–10009.
- 35 *CRC Handbook of Chemistry and Physics*, ed. W. M. Haynes, Taylor and Francis Group, 95th edn, 2014, ISBN: 1-4822-0867-9.
- 36 D. Rehm and A. Weller, *Isr. J. Chem.*, 1970, **8**, 259–271.